One-way quantum computation with two-photon multiqubit cluster states

Giuseppe Vallone,[1,*] Enrico Pomarico,[1,†] Francesco De Martini,[1,2,*] and Paolo Mataloni[1,*]
[1]*Dipartimento di Fisica dell'Universitá Sapienza di Roma and Consorzio Nazionale Interuniversitario per le Scienze Fisiche della Materia, Roma, 00185 Italy*
[2]*Accademia Nazionale dei Lincei, via della Lungara 10, Roma 00165, Italy*
(Received 24 July 2008; published 30 October 2008)

We describe the application of four-qubit cluster states, built on the simultaneous entanglement of two photons in the degrees of freedom of polarization and linear momentum, for the realization of a complete set of basic operations of one-way quantum computation. These consist of arbitrary single-qubit rotations, either probabilistic or deterministic, and simple two-qubit gates, such as a controlled-NOT (CNOT) gate for equatorial qubits and a universal controlled-phase gate (controlled-*Z* or CZ) gate acting on arbitrary target qubits. Other basic computation operations, such as the Grover's search and the Deutsch's algorithms, have been realized by using these states. In all the cases we obtained a high value of the operation fidelities. These results demonstrate that cluster states of two photons entangled in many degrees of freedom are good candidates for the realization of more complex quantum computation operations based on a larger number of qubits.

DOI: 10.1103/PhysRevA.78.042335 PACS number(s): 03.67.Mn, 03.67.Lx

I. INTRODUCTION

The relevance of cluster states in quantum information and quantum computation (QC) has been emphasized in several papers in recent years [1–11]. By these states significant tests of quantum nonlocality, which are more resistant to noise and show significantly larger deviations from classical bounds can be realized [4,12–14].

Besides that, cluster states represent also the basic resource for the realization of a quantum computer operating in the one-way model [1]. In the standard QC approach any quantum algorithm can be realized by a sequence of single-qubit rotations and two-qubit gates, such as controlled-NOT (CNOT) and controlled-PHASE (CPHASE) on the physical qubits [15–17], while deterministic one-way QC is based on the initial preparation of the physical qubits in a cluster state, followed by a temporally ordered pattern of single-qubit measurements and feed-forward (FF) operations [1]. By exploiting the correlations existing between the physical qubits, unitary gates on the so-called "encoded" (or logical) qubit [5] are realized. In this way, nonunitary measurements on the physical qubits correspond to unitary gates on the logical qubits. It is precisely this nonunitarity of the physical process that causes the irreversibility nature (i.e., its "one-way" character) of the model. Hence the difficulties of standard QC, related to the implementation of two qubit gates, are transferred to the preparation of the state.

The FF operations that depend on the outcomes of the already measured qubits and are necessary for a deterministic computation, can be classified in two classes:

The intermediate *feed-forward measurements*, consisting of the choice of the measurement basis.

The Pauli matrix *feed-forward corrections* on the final output state.

The first experimental demonstrations of one-way QC, either probabilistic or deterministic, were given by using four-photon cluster states generated via postselection by spontaneous parametric down conversion (SPDC) [5,8]. The detection rate in those experiments, approximately 1 Hz, was limited by the fact that four-photon events in a standard SPDC process are rare. Moreover, four-photon cluster states are characterized by limited values of fidelity, while efficient computation requires the preparation of highly faithful states.

More recently, by entangling two photons in more degrees of freedom, we created four-qubit cluster states at a much higher level of brightness and fidelity [14]. Precisely, this was demonstrated by entangling the polarization (π) and linear momentum ($\mathbf{k}$) degrees of freedom of one of the two photons belonging to a hyperentangled state [18,19]. Moreover, the possibility of working with only two photons reduces the problems related to the limited quantum efficiency of detectors. Because of these characteristics, two-photon four-qubit cluster states are suitable for the realization of high speed one-way QC [20–22].

In this paper we give a detailed description of the basic QC operations performed by using two-photon four-qubit cluster state, such as arbitrary single qubit rotations, the CNOT gate for equatorial qubits and a CPHASE gate. We verified also the equivalence existing between the two degrees of freedom for qubit rotations, by using either $\mathbf{k}$ or π as the output qubit. Finally, we also show the realization of two important basic algorithms by our setup, namely the Grover's search algorithm and the Deutsch's algorithm. The former identifies the item tagged by a "black box," while the latter allows to distinguish in a single run if a function is *constant* or *balanced*.

The paper is organized as follows. In Sec. II we review the one-way model of QC realized through single-qubit measurements on a cluster state. We also describe the basic building blocks that can be used to implement any general algorithm. In Sec. III a description of the source used to generate the two-photon four-qubit cluster state by manipulating a polarization-momentum hyperentangled state is presented. We describe in Sec. IV three basic operations realized

*URL: http://quantumoptics.phys.uniroma1.it/
†Present address: Univ. de Genève GAP-Optique, Rue de l'École-de-Mèdecine 20, CH-1211 Genève 4, Switzerland.

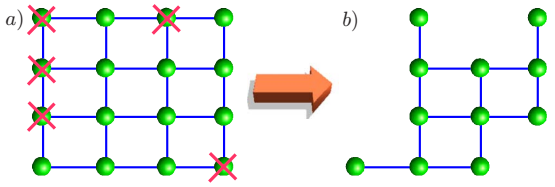

FIG. 1. (Color online). Effect of measurements on a generic cluster state. (a) Measurements in the computational basis $\{|0\rangle, |1\rangle\}$ are indicated by red crosses. (b) The cluster state after the measurements of some qubits in the computational basis.

by our setup: a generic single qubit rotation, a CNOT gate for equatorial target qubit and a CPHASE gate for fixed control and arbitrary target qubit. In Sec. V two explicit examples of quantum computation are given by the realization of the Grover's search algorithm and the the Deutsch's algorithm. Finally, the future perspectives of this research are discussed in the conclusions of Sec. VI.

II. ONE-WAY COMPUTATION

Cluster states are quantum states associated to n-dimensional lattices that, in the case $n=2$ represent a universal resource for QC [23]. The explicit expression of a cluster state is found by associating to each dot j of the lattice (see Fig. 1) a qubit in the state $|+\rangle_j=\frac{1}{\sqrt{2}}(|0\rangle_j+|1\rangle_j)$ and to each link between two adjacent qubits i and j, a CPHASE gate CZ_{ij}:

$$\mathrm{CZ}_{ij}=|0\rangle_i\langle 0|\otimes \mathbb{1}_j+|1\rangle_i\langle 1|\otimes \sigma_z^{(j)}. \tag{1}$$

In the case of a lattice $\mathcal{L}$ with N sites, the corresponding cluster state is given by the expression

$$|\Phi_N^{\mathcal{L}}\rangle \equiv \left(\prod_{i,j \text{ linked}} \mathrm{CZ}_{ij}\right)|+\rangle^N, \tag{2}$$

where $|+\rangle^N\equiv|+\rangle_1\otimes|+\rangle_2\cdots\otimes|+\rangle_N$. Some explicit examples of cluster states are the three-qubit linear cluster,

$$|\Phi_3^{\mathrm{lin}}\rangle=\frac{1}{\sqrt{2}}(|+\rangle_1|0\rangle_2|+\rangle_3+|-\rangle_1|1\rangle_2|-\rangle_3), \tag{3}$$

the four-qubit linear (or horseshoe) cluster

$$\begin{aligned}|\Phi_4^{\mathrm{lin}}\rangle&=|\Phi_4^{\subset}\rangle=|\Phi_4^{\supset}\rangle\\&=\frac{1}{2}(|+\rangle_1|0\rangle_2|0\rangle_3|+\rangle_4+|+\rangle_1|0\rangle_2|1\rangle_3|-\rangle_4\\&\quad+|-\rangle_1|1\rangle_2|0\rangle_3|+\rangle_4+|-\rangle_1|1\rangle_2|1\rangle_3|-\rangle_4),\end{aligned} \tag{4}$$

corresponding to four qubits linked in a row [see Fig. 4(I)] and the four-qubit box cluster

$$\begin{aligned}|\Phi_4^{\square}\rangle&=\frac{1}{2}(|0\rangle_1|+\rangle_2|0\rangle_3|+\rangle_4+|0\rangle_1|-\rangle_2|1\rangle_3|-\rangle_4\\&\quad+|1\rangle_1|-\rangle_2|0\rangle_3|-\rangle_4+|1\rangle_1|+\rangle_2|1\rangle_3|+\rangle_4),\end{aligned} \tag{5}$$

corresponding to four qubits linked in a square [see Fig. 10 (left)].

For a given cluster state, the measurement of a generic qubit j performed in the computational basis $\{|0\rangle_j,|1\rangle_j\}$ [Fig. 1(a)] simply corresponds to remove it and its relative links from the cluster [Fig. 1(b)]. In this way we obtain, up to possible σ_z corrections, a cluster state with $N-1$ qubits,

$$|\Phi_N^{\mathcal{L}}\rangle \to \prod_{k\in\mathcal{N}_j}(\sigma_z^{(k)})^{s_j}|\Phi_{N-1}^{\mathcal{L}\setminus\{j\}}\rangle, \tag{6}$$

where $s_j=0$ if the measurement output is $|0\rangle_j$, while $s_j=1$ if the measurement output is $|1\rangle_j$. In the previous equation $\mathcal{N}_j$ stands for the set of all sites linked with qubit j. Then, by starting from a large enough square lattice, it is possible to create any kind of cluster state associated to smaller lattices. In the following figures we will indicate with a red cross the measurement of a physical qubit performed in the computational basis, as shown in Fig. 1.

Let us now explain the computation process. Each algorithm consists of a measurement pattern on a specific cluster state. This pattern has a precise temporal ordering. It is well known that one-way computation does not operate directly on the physical qubits of the cluster state on which measurements are performed. The actual computation takes place on the so-called encoded qubits, written nonlocally in the cluster through the correlation between physical qubits. We will use $i,j=1,\ldots,N$ for the physical qubits and $a,b=1,\ldots,M$ for the encoded qubits ($M<N$). Some physical qubits (precisely M) represent the input qubits of the computation (all prepared in the state $|+\rangle_E$) and the corresponding dots can be arranged at the left of the graph. We then measure $N-M$ qubits, leaving M physical qubits unmeasured, hence the output of computation corresponds (up to Pauli errors) to the unmeasured qubits. It is possible to arrange the position of the dots in such a way that the time ordering of the measurement pattern goes from left to right.

The computation proceeds by the measurement performed in the basis

$$B_j(\varphi)\equiv\{|\varphi_+\rangle_j,|\varphi_-\rangle_j\}, \tag{7}$$

where $|\varphi_\pm\rangle_j\equiv\frac{1}{\sqrt{2}}(e^{i\varphi/2}|0\rangle_j\pm e^{-i\varphi/2}|1\rangle_j)$. Here $s_j=0$ or $s_j=1$ if the measurement outcome of qubit j is $|\varphi_+\rangle_j$ or $|\varphi_-\rangle_j$, respectively. The specific choice of φ for every physical qubit is determined by the measurement pattern. Note that the choice of the measurement basis for a specific qubit can also depend on the outcome of the already measured qubits: these are what we call feed-forward measurements [type (i)]. In general, active modulators (for example, Pockels cells in case of polarization qubit) are required to perform FF measurements. However, in some cases, when more than one qubit is encoded in the same particle through different degrees of freedom (DOF's), it is possible to perform FF measurement without the need of active modulators. This will be discussed in Sec. IV, when the measurement basis of the generic qubit j, encoded in one particle, depends only on the outputs of some other qubits encoded in the same particle.

One-way computation can be understood in terms of some basic operations, the so-called cluster building blocks (CBB) (see Fig. 2). By combining different CBB it is possible to realize computation algorithms of arbitrary complexity [24]. We introduce here a convenient notation: by writing explic-

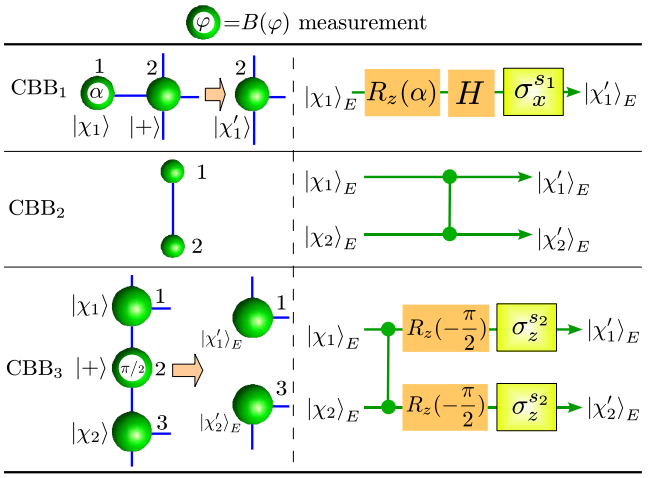

FIG. 2. (Color online). Cluster building blocks (CBB). For each CBB_i we indicate the measurement on the physical cluster (left) and the corresponding operation on the logical qubits (right).

itly a state $|\chi\rangle$ close to a dot j (see Fig. 2), we indicate that the total state could be equivalently obtained by preparing qubit j in the state $|\chi\rangle_j$ before applying the necessary CZ gates.

CBB_1: Qubit rotation. Consider two qubits linked together like CBB_1 shown in Fig. 2. Here the first qubit is initially prepared in the state $|\chi\rangle$ and the second qubit is arbitrary linked with other dots. By measuring qubit 1 in the basis $B_1(\alpha)$ we remove it from the cluster but we transfer the information into qubit 2 leaving its links unaltered. This corresponds to the following operation on the encoded qubit $|\chi\rangle_E$

$$|\chi\rangle_E \to |\chi'\rangle_E \equiv \sigma_x^{s_1} H R_z(\alpha)|\chi\rangle_E, \tag{8}$$

where H is the Hadamard gate $H=1/\sqrt{2}(\sigma_x+\sigma_z)$ and $R_z(\alpha)=e^{-i\alpha\sigma_z/2}$ is a rotation around the z axis in the Bloch sphere. The σ_x operations depends on the measurement output (s_1) of the first qubit. This operation can be understood by noting that by measuring the first qubit of the state $\mathrm{CZ}_{12}|\chi\rangle_1|+\rangle_2$ in the $B_1(\alpha)$ basis we obtain $|\chi'\rangle_2$.

This simple algorithm can be repeated by using two CBB_1 in a row. By measuring qubit 1 in the $B_1(\alpha)$ bases the encoded qubit is transformed into $|\chi'\rangle_E$ and the encoded qubit moves from left to right within the cluster. By measuring qubit 2 in the $B_2(\beta)$ basis the encoded qubit is now written in qubit 3 as $|\chi''\rangle_E$,

$$|\chi''\rangle_E \equiv \sigma_x^{s_2} H R_z(\beta)\sigma_x^{s_1} H R_z(\alpha)|\chi\rangle_E. \tag{9}$$

In this case the computation can be understood by observing that by the measurement of qubits 1 and 2 of the state $\mathrm{CZ}_{12}\mathrm{CZ}_{23}|\chi\rangle_1|+\rangle_2|+\rangle_3$ in the basis $B_1(\alpha)$ and $B_2(\beta)$, we obtain $|\chi''\rangle_3$.

CBB_2: CPHASE *gate*. Consider two qubits linked in a column. This block simply performs a CPHASE gate (CZ) between the two qubits.

CBB_3: CPHASE *gate+rotation*. With three qubits in a column, the measurement of the second qubit in the basis $B_2(\pi/2)$ is equivalent to remove it from the cluster and to transfer the information to qubits 1 and 3. Precisely, this measurement realizes a CPHASE gate followed by two single-qubit rotations $R_z(-\pi/2)$ on the logical qubit (see Fig. 2).

By combining these CBB we can obtain any desired quantum algorithm, expressed in general as

$$|\psi_{out}\rangle = U_\Sigma U_g \prod_{a=1}^{M} |+\rangle_a, \tag{10}$$

where M is the number of logical qubits, U_g is the unitary gate that the algorithm must perform, and U_Σ correspond to the so-called Pauli errors corrections [24,25],

$$U_\Sigma = \prod_{a=1}^{M} (\sigma_x^{[a]})^{x_a} (\sigma_z^{[a]})^{z_a}. \tag{11}$$

The numbers x_a, $z_a=0,1$ depend on the outcomes of all the single (physical) qubit measurements and determine the FF corrections [type (ii)] that must be realized at the end of the measurement pattern to achieve deterministic computation. By the symbol $\sigma_z^{[a]}$ we indicate that the Pauli matrix σ_z acts on the logical qubit a. Note that if the output of the algorithm is one among the 2^M states of the computational basis, i.e., $\otimes_{a=1}^{M}|r_a\rangle_a$ $(r_a=0,1)$, only the σ_x's of the unitary U_Σ act non-trivially by flipping some qubits. The Pauli errors are then reduced to

$$U'_\Sigma = \prod_{a=1}^{M} (\sigma_x^{[a]})^{x_a}. \tag{12}$$

In this way the "errors" can be simply corrected by relabeling the output, and with no need of active feed-forward corrections on the quantum state. If, by measuring the output qubits, we obtain the result $\Pi_{a=1}^{M}|s_a\rangle_a$ ($s_a=0$ or $s_a=1$) we must interpret it as $\Pi_{a=1}^{M}|s_a \oplus x_a\rangle_a$ with the Pauli errors given by Eq. (12). This relabeling operation can be performed, for example, by an external classical computer.

III. EXPERIMENTAL SETUP

In our experiment we generated two-photon four-qubit cluster states by starting from polarization (π)-momentum $(\mathbf{k})$ hyperentangled photon pairs obtained by SPDC (see Fig. 3). The hyperentangled states $|\Xi^{\pm\pm}\rangle \equiv |\Phi^{\pm}\rangle_\pi \otimes |\psi^{\pm}\rangle_{\mathbf{k}}$ were generated by a β-barium-borate (BBO) type-I crystal pumped in both sides by a cw Argon laser beam ($\lambda_p=364$ nm) (see Fig. 3). The detailed explanation of the hyperentangled state preparation was given in previous papers [18,26], to which we refer for details. In the above expression of $|\Xi^{\pm\pm}\rangle$ we use the Bell states

$$|\Phi^{\pm}\rangle_\pi = \frac{1}{\sqrt{2}}(|H\rangle_A|H\rangle_B \pm |V\rangle_A|V\rangle_B),$$

$$|\psi^{\pm}\rangle_{\mathbf{k}} = \frac{1}{\sqrt{2}}(|\ell\rangle_A|r\rangle_B \pm |r\rangle_A|\ell\rangle_B), \tag{13}$$

with $|H\rangle, |V\rangle$ corresponding to the horizontal (H) and vertical (V) polarization and $|\ell\rangle, |r\rangle$ referring to the left (ℓ) or right

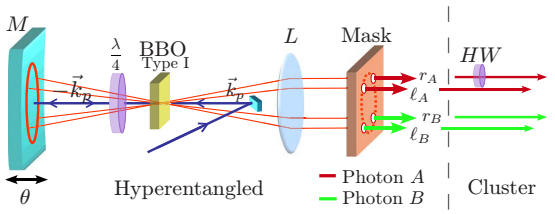

FIG. 3. (Color online) Source of two-photon four-qubit cluster state. The hyperentangled states $|\Xi^{\pm\pm}\rangle$ arises from the simultaneous entanglement on polarization and linear momentum. Polarization entanglement is obtained by pumping in two opposite directions a BBO type-I crystal and by double passage of the SPDC pair through a $\lambda/4$ wave plate. Mode selection performed by a four hole screen allows linear momentum entanglement. The half wave plate HW transforms the hyperentangled state $|\Xi^{+-}\rangle$ into the cluster state $|C_4\rangle$.

(r) paths of the photon A (Alice) or B (Bob) (see Fig. 3). In $|\Xi^{\pm\pm}\rangle$, the first signs refer to the polarization state $|\phi^{\pm}\rangle_{\pi}$ and the second ones to the linear momentum state $|\psi^{\pm}\rangle_{\mathbf{k}}$.

Starting from the state $|\Xi^{+-}\rangle=|\Phi^{+}\rangle_{\pi}\otimes|\psi^{-}\rangle_{\mathbf{k}}$ and applying a CPHASE (CZ) gate between the control $(\mathbf{k_A})$ and the target (π_A) qubits of photon A, the cluster state

$$\begin{aligned}|C_4\rangle &= \frac{1}{2}(|H\ell\rangle_A|Hr\rangle_B - |Hr\rangle_A|H\ell\rangle_B + |Vr\rangle_A|V\ell\rangle_B \\ &\quad + |V\ell\rangle_A|Vr\rangle_B) \\ &= \frac{1}{\sqrt{2}}|\Phi^{+}\rangle_{\pi}|\ell\rangle_A|r\rangle_A - \frac{1}{\sqrt{2}}|\Phi^{-}\rangle_{\pi}|r\rangle_A|\ell\rangle_A \\ &= \frac{1}{\sqrt{2}}|H\rangle_A|H\rangle_A|\psi^{+}\rangle_{\mathbf{k}} + \frac{1}{\sqrt{2}}|V\rangle_A|V\rangle_A|\psi^{-}\rangle_{\mathbf{k}} \end{aligned} \tag{14}$$

is generated. In the experiment, the CZ gate is realized by a zero-order half wave (HW) plate inserted on the r_A mode, and corresponds to introduce a π phase shift on the vertical polarization of the r_A output mode. It is worth noting that, at variance with the case of four-photon cluster states, the state (14) is created without any kind of postselection [33]. By using the correspondence $|H\rangle\leftrightarrow|0\rangle$, $|V\rangle\leftrightarrow|1\rangle$, $|\ell\rangle\leftrightarrow|0\rangle$, $|r\rangle\leftrightarrow|1\rangle$, the generated state $|C_4\rangle$ is equivalent to $|\Phi_4^{\mathrm{lin}}\rangle$, $|\Phi_4^{\subset}\rangle$, $|\Phi_4^{\supset}\rangle$, or $|\Phi_4^{\square}\rangle$ up to single qubit unitaries,

$$|C_4\rangle = U_1\otimes U_2\otimes U_3\otimes U_4|\Phi_4^{\mathrm{lin}}\rangle \equiv \mathcal{U}|\Phi_4^{\mathrm{lin}}\rangle. \tag{15}$$

With $|\Phi_4^{\mathrm{lin}}\rangle$ and $|C_4\rangle$ we refer to the cluster state expressed in the "cluster" and "laboratory" basis, respectively. The explicit expression of the unitaries U_j depends on the specific ordering of the physical qubits ($\mathbf{k_A}$, $\mathbf{k_B}$, π_A, and π_B) and in the following will be indicated in each case. The change of basis is necessary to know which are the correct measurements needed in the actual experiment. In general, if the chosen algorithm requires a measurement in the basis $|\alpha_{\pm}\rangle_j$ on qubit j, the actual measurement basis in the laboratory is given by $U_j|\alpha_{\pm}\rangle_j$.

In order to characterize the generated cluster state we adopted the stabilizer operator formalism [27]. It can be shown [28] that

TABLE I. Expectation values of the stabilizer operators S_i.

	Stabilizers	$\mathrm{Tr}[\rho_{exp}S_k]$
S_1	$-z_Az_B$	0.9941 ± 0.0011
S_2	$-x_Ax_BZ_A$	0.8486 ± 0.0031
S_3	$z_AX_AX_B$	0.9372 ± 0.0035
S_4	Z_AZ_B	0.9105 ± 0.0024
S_5	$-y_Ay_BZ_A$	0.8386 ± 0.0032
S_6	$-z_BX_AX_B$	0.9354 ± 0.0035
S_7	$-Z_AZ_Bz_Az_B$	0.8963 ± 0.0044
S_8	$Y_AX_Bx_Ay_B$	0.7455 ± 0.0042
S_9	$-Z_By_Ay_B$	0.8215 ± 0.0034
S_{10}	$X_AY_Bx_AY_B$	0.8139 ± 0.0037
S_{11}	$-Y_AX_By_Ax_B$	0.7944 ± 0.0037
S_{12}	$-x_Ax_BZ_B$	0.8498 ± 0.0031
S_{13}	$-Y_AY_Bz_A$	0.9350 ± 0.0036
S_{14}	$Y_AY_Bz_B$	0.9346 ± 0.0037
S_{15}	$-X_AY_By_Ax_B$	0.8186 ± 0.0035
S_{16}	$\mathbb{1}$	1

$$|C_4\rangle\langle C_4| = \frac{1}{16}\sum_{k=1}^{16} S_k, \tag{16}$$

where S_k are the so-called *stabilizer operators* $S_k|C_4\rangle=|C_4\rangle$, $\forall k=1,\ldots,16$ (see Table I). The fidelity of the experimental cluster ρ_{exp} can be measured by

$$F_{|C_4\rangle} = \mathrm{Tr}[\rho_{exp}|C_4\rangle\langle C_4|] = \frac{1}{16}\sum_{k=1}^{16}\mathrm{Tr}[\rho_{exp}S_k], \tag{17}$$

i.e., by measuring the expectation values of the stabilizer operators. We show in Table I the stabilizer operators for $|C_4\rangle$ and the corresponding experimental expectation values. The measured fidelity was $F=0.880\pm0.013$, demonstrating the high purity level of the generated state. Cluster states were observed at 1 kHz detection rate by using interference filters with bandwidth $\Delta\lambda=6$ nm for photon pair detection. In Table I we use the following notation for polarization:

$$\begin{aligned} Z_j &= |H\rangle_j\langle H| - |V\rangle_j\langle V|, \\ Y_j &= i|V\rangle_j\langle H| - i|H\rangle_j\langle V|, \\ X_j &= |H\rangle_j\langle V| + |V\rangle_j\langle H|, \quad j=A,B, \end{aligned} \tag{18}$$

and linear momentum operators

$$\begin{aligned} z_j &= |\ell\rangle_j\langle\ell| - |r\rangle_j\langle r|, \\ y_j &= i|r\rangle_j\langle\ell| - i|\ell\rangle_j\langle r|, \\ x_j &= |\ell\rangle_j\langle r| + |r\rangle_j\langle\ell|, \quad j=A,B, \end{aligned} \tag{19}$$

for either Alice (A) or Bob (B) photons.

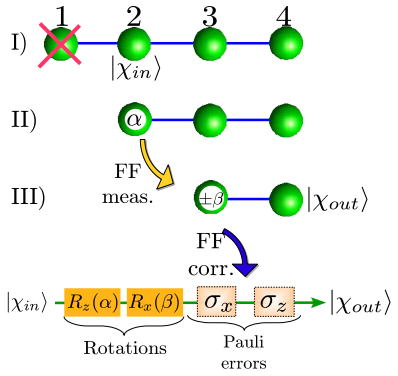

FIG. 4. (Color online) Measurement pattern for single-qubit rotations. Top: Arbitrary single-qubit rotations on a four-qubit linear cluster state are carried out in three steps (I, II, III). In each measurement, indicated by a red cross, the information travels from left to right. Bottom: Equivalent logical circuit.

IV. BASIC OPERATIONS WITH TWO-PHOTON CLUSTER STATE

In this section we describe the implementation of simple operations performed by the generated four-qubit two-photon cluster state.

A. Single-qubit rotations

In the one-way model a three-qubit linear cluster state (simply obtained by the four-qubit cluster by measuring the first qubit) is sufficient to realize an arbitrary single-qubit transformation [34] $|\chi_{in}\rangle \rightarrow R_x(\beta)R_z(\alpha)|\chi_{in}\rangle$, where $R_z(\alpha) = e^{-i\alpha\sigma_z/2}$ and $R_x(\beta) = e^{-i\beta\sigma_x/2}$.

The algorithm consists of two CCB_1 on a row. Precisely, by using the four-qubit cluster expressed in the cluster basis the following measurement pattern must be followed (see Fig. 4):

(1) A three-qubit linear cluster is generated by measuring the first qubit in the computational basis $\{|0\rangle_1, |1\rangle_1\}$. As already stated in Sec. II this operation removes the first qubit from the cluster and generates $(\sigma_z^{(2)})^{s_1}|\Phi_3^{\text{lin}}\rangle$. The input logical qubit $|\chi_{in}\rangle$ is then encoded in qubit 2. If the outcome of the first measurement is $|0\rangle_1$ then $|\chi_{in}\rangle = |+\rangle$, otherwise $|\chi_{in}\rangle = |-\rangle$.

(II) Measuring qubit 2 in the basis $B_2(\alpha)$, the logical qubit (now encoded in qubit 3) is transformed into $|\chi'\rangle = (\sigma_x)^{s_2} H R_z(\alpha)|\chi_{in}\rangle$, with $R_z(\alpha) = e^{-(i/2)\alpha\sigma_z}$.

(III) Measurement of qubit 3 is performed in the basis

$$B_3(\beta) \quad \text{if } s_2 = 0,$$

$$B_3(-\beta) \quad \text{if } s_2 = 1.$$

This represents a FF measurement [type (i)] since the choice of measurement basis depends on the previous outputs. This operation leaves the last qubit in the state $|\chi_{out}\rangle = (\sigma_x)^{s_3} H R_z[(-1)^{s_2}\beta]|\chi'\rangle$.

The above sequence indicates that the measurement result in each step determines the measurement basis in the subsequent steps. Hence, in the case of two-photon, four-qubit cluster states, when more qubits are encoded in a single photon, the process proceeds in a determinstic way thanks to the FF measurements. At the end of the process, by using some simple Pauli matrix algebra, the output state (encoded in qubit 4) can be written as

$$|\chi_{out}\rangle = \sigma_x^{s_3}\sigma_z^{s_2} R_x(\beta)R_z(\alpha)|\chi_{in}\rangle. \tag{20}$$

with $R_x(\beta) = e^{-(i/2)\beta\sigma_x}$. In this way, by suitable choosing α and β, we can perform any arbitrary single-qubit rotation $|\chi_{in}\rangle \rightarrow R_x(\beta)R_z(\alpha)|\chi_{in}\rangle$ up to Pauli errors $(\sigma_x^{s_3}\sigma_z^{s_2})$ that should be corrected by proper feed-forward operations [type (ii)] to achieve a deterministic computation [8].

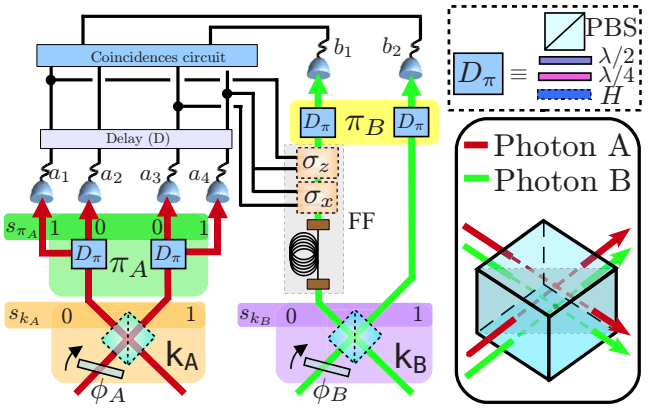

FIG. 5. (Color online) Measurement setup for photons A and B. Momentum qubits $\mathbf{k_A}$ and $\mathbf{k_B}$ are measured by two thin glasses (ϕ_A, ϕ_B), acting as phase shifters and inserted before a common 50:50 BS. Polarization qubits π_A and π_B are measured by standard tomographic setup (D_π). BS and D_π outputs are indicated by $s_j = 0, 1$, where the index j refers to the corresponding DOF. FF correction apparatus for deterministic QC [used in our experiment only with ordering (a)] is given by a 35 m length single mode fiber and two Pockels cells (σ_x, σ_z) driven by the output signals of detector a_1, a_3, a_4. Dashed lines for H, BS, and FF correction apparatus indicate that these devices can be inserted or not in the setup depending on the particular measurement (see text for details). Inset: tomographic apparatus D_π and spatial mode matching on the BS.

In our case we applied this measurement pattern by considering different ordering of the physical qubits. Precisely, we encoded the output qubit either in polarization or linear momentum of photon B, demonstrating the QC computational equivalence of the two DOF's. The measurement apparatus is sketched in Fig. 5. The $\mathbf{k}$ modes corresponding to photons A or B are matched respectively, on the up and down side of a common symmetric beam splitter (BS) (see inset), which also can be finely adjusted in the vertical direction such that one or both photons don not pass through it. Polarization analysis is performed by a standard quantum tomography apparatus D_π ($\lambda/4$, $\lambda/2$, and polarizing beam splitter PBS). Depending of the specific measurement the HWs oriented at 22.5° are inserted to perform the Hadamard operation H in the apparatus D_π. They are used together with the $\lambda/4$ in order to transform the $\{|\varphi_+\rangle_{\pi_A}, |\varphi_-\rangle_{\pi_A}\}$ states into linearly polarized states. Two thin glass plates before the BS allow to set the basis of the momentum measurement for each photon.

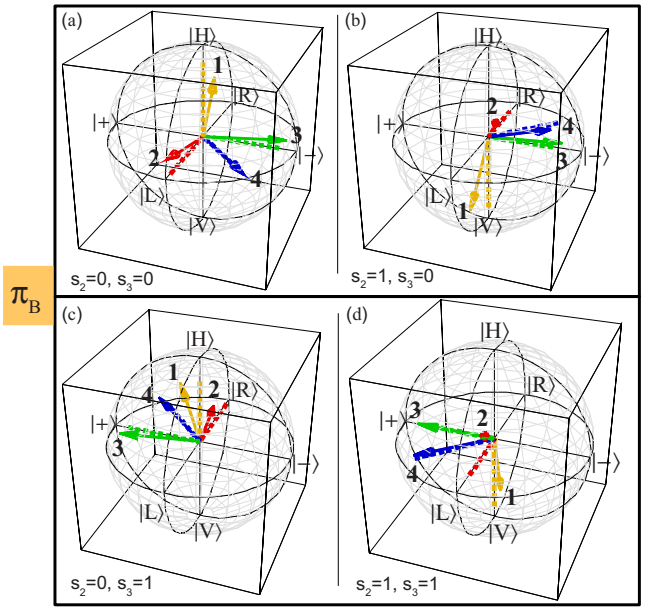

FIG. 6. (Color online) Polarization (π_B) output Bloch vectors of single-qubit rotations. The experimental results (arrows) are shown with their projections on theoretical directions (dashed lines). Arrow colors correspond to different values of α and β (see Table II).

Let us consider the following ordering of the physical qubits [see Eq. (15)]:

$$\text{(a)} \quad (1,2,3,4) = (\mathbf{k}_B, \mathbf{k}_A, \pi_A, \pi_B),$$

$$\mathcal{U} = \sigma_x H \otimes \sigma_z \otimes \mathbb{1} \otimes H. \tag{21}$$

The output state, encoded in the polarization of photon B, can be written in the laboratory basis as

$$|\chi_{out}\rangle_{\pi_B} = \sigma_z^{s_{\pi_A}} \sigma_x^{s_{\mathbf{k}_A}} H R_x(\beta) R_z(\alpha) |\chi_{in}\rangle, \tag{22}$$

where the H gate derives from the change between the cluster and laboratory basis. This also implies that the actual measurement bases are $B_{\mathbf{k}_B}(0)$ for the momentum of photon B (qubit 1) and $B_{\mathbf{k}_A}(\alpha+\pi)$ (i.e., $|\alpha_{\mp}\rangle_{\mathbf{k}_A}$) for the momentum of photon A (qubit 2). According to the one-way model, the measurement basis on the third qubit (π_A) depends on the results of the measurement on the second qubit ($\mathbf{k}_A$). These are precisely what we call FF measurements [type (i)]. In our scheme this simply corresponds to measure π_A in the bases $B_{\pi_A}(\beta)$ or $B_{\pi_A}(-\beta)$, depending on the BS output mode (i.e., $s_{\mathbf{k}_A}=0$ or $s_{\mathbf{k}_A}=1$). These deterministic FF measurements are a direct consequence of the possibility to encode two qubits ($\mathbf{k}_A$ and π_A) in the same photon. As a consequence, at variance with the case of four-photon cluster states, in this case active feed-forward measurements (that can be realized by adopting Pockels cells) are not required, while Pauli errors corrections are in any case necessary for deterministic QC.

We first realized the experiment without FF corrections (in this case we did not use the retardation fiber and the Pockels cells shown in the setup). The results obtained for $s_2=s_3=0$ (i.e., when the computation proceeds without errors) with $|\chi_{in}\rangle=|+\rangle$ are shown in Fig. 6(a). We show on the Bloch sphere the experimental output qubits and their projections on the theoretical state $HR_x(\beta)R_z(\alpha)|+\rangle$ for the whole set of α and β. The corresponding fidelities are given in Table II. We also performed the tomographic analysis [shown in Figs. 6(b)–6(d)] on the output qubit π_B for all the possible combinations of s_2 and s_3 and for the input qubit $|\chi_{in}\rangle=|\pm\rangle$. The high fidelities obtained in these measurements indicate that deterministic QC can be efficiently implemented in this configuration by Pauli error active FF corrections.

They were realized by using the entire measurement apparatus of Fig. 5. Here two fast driven transverse $LiNbO_3$ Pockels cells (σ_x and σ_z) with risetime=1 ns and $V_{\lambda/2} \sim 1$ kV are activated by the output signals of detectors a_i ($i=1,3,4$) corresponding to the different values of s_{π_A} and $s_{\mathbf{k}_A}$. They perform the operation $\sigma_z^{s_{\pi_A}}\sigma_x^{s_{\mathbf{k}_A}}$ on photon B, coming from the output $s_{\mathbf{k}_B}=0$ of BS and transmitted through a single mode optical fiber. Note that no correction is needed when photon A is detected on the output a_2 ($s_{\pi_A}=s_{\mathbf{k}_A}=0$). Temporal synchronization between the activation of the high voltage signal and the transmission of photon B through the Pockels cells is guaranteed by suitable choice of the delays

TABLE II. Polarization (π_B) experimental fidelities (F) of single-qubit rotation output states for different values of α and β. The first column indicates the corresponding vector in Fig. 6. Each datum is obtained by the measurements of the different Stokes parameters, each one lasting 10 s.

	No.	α	β	F $(s_2=0,s_3=0)$	F $(s_2=0,s_3=1)$
	1	0	$\pi/2$	0.908 ± 0.006	0.860 ± 0.008
π_B	**2**	$-\pi/2$	0	0.942 ± 0.004	0.946 ± 0.004
	3	$-\pi/2$	$\pi/2$	0.913 ± 0.005	0.929 ± 0.004
	4	$-\pi/2$	$-\pi/4$	0.899 ± 0.007	0.898 ± 0.006
	No.	α	β	F $(s_2=1,s_3=0)$	F $(s_2=1,s_3=1)$
	1	0	$\pi/2$	0.932 ± 0.005	0.935 ± 0.006
π_B	**2**	$-\pi/2$	0	0.873 ± 0.006	0.847 ± 0.006
	3	$-\pi/2$	$\pi/2$	0.851 ± 0.007	0.848 ± 0.007
	4	$-\pi/2$	$-\pi/4$	0.928 ± 0.007	0.932 ± 0.007

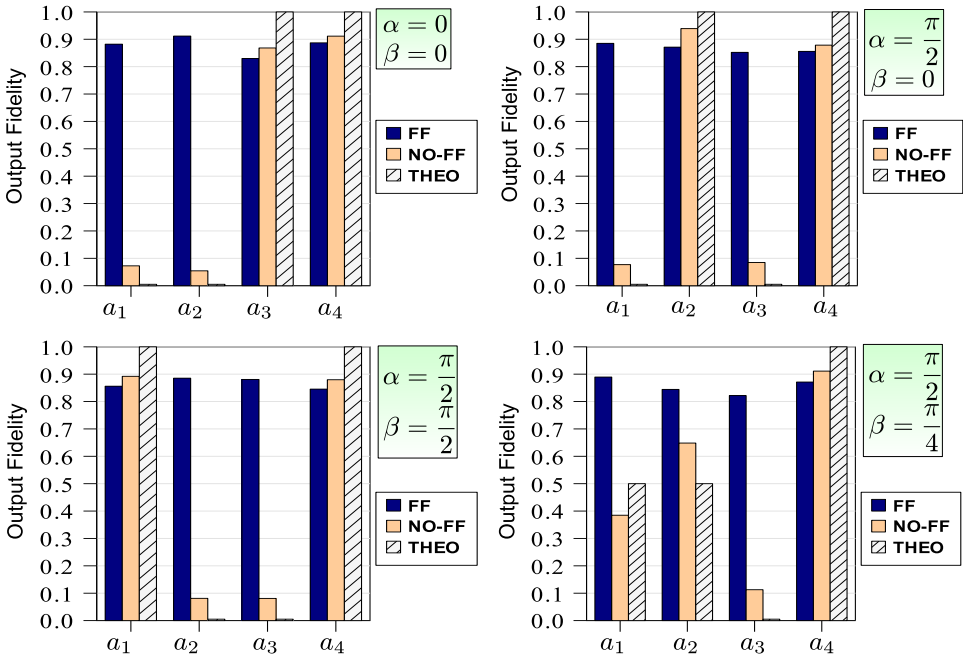

FIG. 7. (Color online) Output fidelities of the single-qubit rotation algorithm with [FF, black (blue) columns] or without [no FF, gray (orange) columns] feed forward. In both cases, the four columns of the histograms refer to the measurement of the output state (encoded in the polarization of photon B) by detector b_1 in coincidence with $a_1,\ldots,a_4$, respectively. Grey dashed columns (THEO) correspond to theoretical fidelities in the no-FF case.

D. We used only one BS output of photon B, namely $s_{\mathbf{k_B}}=0$, in order to perform the algorithm with initial state $|\chi_{in}\rangle=|+\rangle$. The other BS output corresponds to the algorithm starting with the initial state $|\chi_{in}\rangle=|-\rangle$. By referring to Fig. 5, each detector a_j corresponds to a different value of $s_{\mathbf{k_A}}$ and s_{π_A}. Precisely, a_1 corresponds to $s_{\mathbf{k_A}}=0$ and $s_{\pi_A}=1$ and activates the Pockels cell σ_z [see Eq. (22)]. Detector a_2 corresponds to $s_{\mathbf{k_A}}=s_{\pi_A}=0$, i.e., the computation without errors and thus no Pockels cell is activated. Detector a_3 corresponds to $s_{\mathbf{k_A}}=1$, $s_{\pi_A}=0$, and activates σ_x, while a_4 corresponds to $s_{\mathbf{k_A}}=s_{\pi_A}=1$ and both σ_x and σ_z are activated.

In Fig. 7 the output state fidelities obtained with and/or without active FF corrections (i.e., turning on and/or off the Pockels cells) are compared for different values of α and β. The expected theoretical fidelities in the no-FF case are also shown. In all the cases the computational errors are corrected by the FF action, with average measured fidelity $F=0.867\pm0.018$. In the experiment the overall repetition rate was about 500 Hz, which is more than two orders of magnitude larger than one-way single qubit-rotation realized with four-photon cluster states.

We also demonstrated the computational equivalence of the two DOF's of photon B by performing the same algorithm with the following qubit ordering:

$$\text{(b)} \quad (1,2,3,4)=(\pi_B,\pi_A,\mathbf{k}_A,\mathbf{k}_B),$$

$$\mathcal{U}=H\otimes\sigma_z\otimes\sigma_x\otimes\sigma_z H. \tag{23}$$

In this case we used the momentum of photon B ($\mathbf{k_B}$) as output state. The explicit expression of the output state $|\chi_{out}\rangle_{\mathbf{k}_B}$ in the laboratory basis is now $|\chi_{out}\rangle_{\mathbf{k}_B}=(\sigma_z)^{s_3}(\sigma_x)^{s_2}\sigma_z HR_x(\beta)R_z(\alpha)|\chi_{in}\rangle$. By using only detectors a_2, a_3, b_1, b_2 in Fig. 5 we measured $|\chi_{out}\rangle_{\mathbf{k}_B}$ for different values of α (which correspond in the laboratory to the polarization measurement bases $|\alpha_{\mp}\rangle_{\pi_A}$) and $\beta=0$ (which correspond in the laboratory to the momentum bases $|-\beta_{\pm}\rangle_{\mathbf{k}_A}$). The first qubit ($\pi_B$) was always measured in the basis $|\pm\rangle_{\pi_B}$. The $\mathbf{k}_B$ tomographic analysis for all the possible values of $s_2\equiv s_{\pi_A}$ and $s_3\equiv s_{\mathbf{k_A}}$ are shown in Fig. 8, i.e., for different values of $s_1\equiv s_{\pi_B}$. We obtained an average value of fidelity $F>0.9$ (see Table III). In this case the realization of deterministic QC by FF corrections could be realized by the adoption of active phase modulators. The (π)-($\mathbf{k}$) computational equivalence and the use of active feed forward show that the multidegree of freedom approach is feasible for deterministic one-way QC.

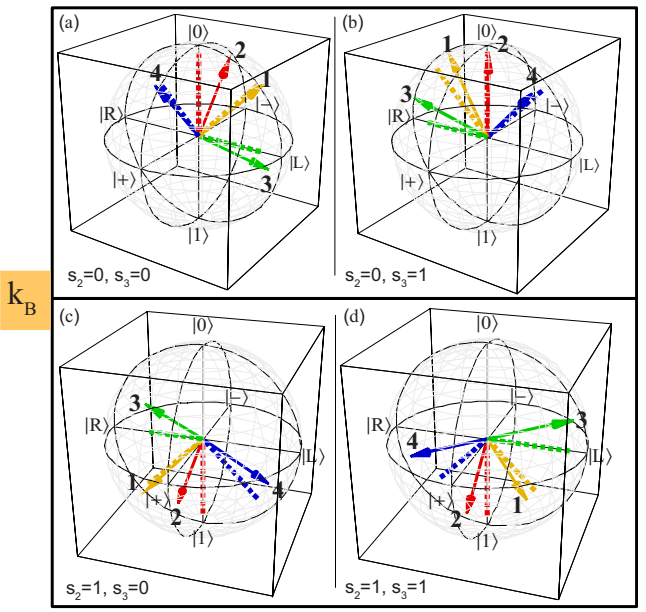

FIG. 8. (Color online) Momentum ($\mathbf{k_B}$) output Bloch vectors of single-qubit rotations. The experimental results (arrows) are shown with their projections on theoretical directions (dashed lines). Arrow colors correspond to different values of α and β (see Table III).

TABLE III. Momentum ($\mathbf{k_B}$) experimental fidelities (F) of single-qubit rotation output states for different values of α and β. The first column indicates the corresponding vector in Fig. 8. Each datum is obtained by the measurements of the different Stokes parameters, each one lasting 10 s.

	No.	$\alpha(\beta=0)$	$F\ (s_2=0,s_3=0)$	$F\ (s_2=0,s_3=1)$
	1	$\pi/4$	0.998 ± 0.005	0.961 ± 0.006
$\mathbf{k_B}$	**2**	0	0.961 ± 0.003	0.971 ± 0.003
	3	$\pi/2$	0.879 ± 0.006	0.895 ± 0.005
	4	$-\pi/4$	0.833 ± 0.007	0.956 ± 0.006
	No.	$\alpha(\beta=0)$	$F\ (s_2=1,s_3=0)$	$F\ (s_2=1,s_3=1)$
	1	$\pi/4$	0.919 ± 0.008	0.857 ± 0.009
$\mathbf{k_B}$	**2**	0	0.944 ± 0.0044	0.943 ± 0.005
	3	$\pi/2$	0.799 ± 0.007	0.918 ± 0.005
	4	$-\pi/4$	0.946 ± 0.008	0.872 ± 0.008

B. C-NOT gate

The four-qubit cluster allows the implementation of nontrivial two-qubit operations, such as the CNOT ($\mathcal{G}_{\mathrm{CNOT}}$) gate. Precisely, a CNOT gate acting on a generic target qubit belonging to the equatorial plane of the Bloch sphere [i.e., a generic state of the form $\frac{1}{\sqrt{2}}(|0\rangle+e^{i\gamma}|1\rangle)$] can be realized by the four-qubit horseshoe (180° rotated) cluster state $|\Phi_4^{\mathrm{lin}}\rangle$ [see Eq. (4)]. Let us consider Fig. 9 (top). The measurement of qubits 1 and 4 realizes a CNOT gate (the logical circuit shown in figure) between the control $|+\rangle_c$ and target $|+\rangle_t$ qubit. By measuring the qubit 1 in the basis $\{|0\rangle_1,|1\rangle_1\}$ or $|\pm\rangle_1$ we realized on the control input qubit $|+\rangle_c$ the gate $\mathcal{O}=\mathbb{1}$ or $\mathcal{O}=H$, respectively. The measurement of qubit 4 in the basis $|\alpha_\pm\rangle_4$ realizes the gate $HR_z(\alpha)$ on the target input qubit $|+\rangle_t$. The algorithm is terminated by the vertical link performing a CZ operation. The input state $|+\rangle_c\otimes|+\rangle_t$ is transformed, in case of no "errors" (i.e., $s_1=s_4=0$), into $|\Psi_{out}\rangle=\mathcal{G}_{\mathrm{CZ}_{ct}}(\mathcal{O}|+\rangle_c\otimes H_tR_z(\alpha)|+\rangle_t)=H_t\mathcal{G}_{\mathrm{CNOT}}(\mathcal{O}|+\rangle_c\otimes R_z(\alpha)|+\rangle_t)$. This circuit realizes the CNOT gate (up to the Hadamard H_t) for arbitrary equatorial target qubit [since

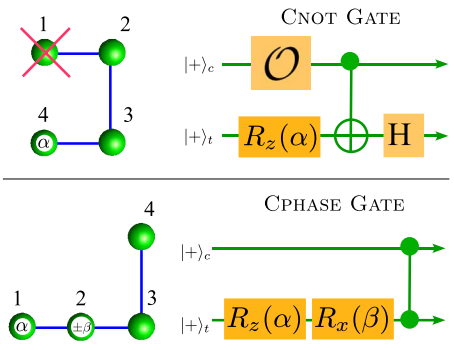

FIG. 9. (Color online) CNOT and CPHASE gates by the four-qubit cluster. (Top) CNOT gate realization via measurement of qubits 1, 4 on the horseshoe cluster and equivalent circuit. (Bottom) CPHASE gate realization via measurement of qubits 1 and 2 in the bases $B_1(\alpha)$ and $B_2(\alpha)$ and equivalent circuit.

TABLE IV. Experimental fidelity (F) of CNOT gate output target qubit for different value of α and $\mathcal{O}$.

$\mathcal{O}$	α	Control output	$F\ (s_4=0)$	$F\ (s_4=1)$
	$\pi/2$	$s_1=0\rightarrow\|1\rangle_c$	0.965 ± 0.004	0.975 ± 0.004
H		$s_1=1\rightarrow\|0\rangle_c$	0.972 ± 0.004	0.973 ± 0.004
	$\pi/4$	$s_1=0\rightarrow\|1\rangle_c$	0.995 ± 0.008	0.902 ± 0.012
		$s_1=1\rightarrow\|0\rangle_c$	0.946 ± 0.010	0.945 ± 0.009
$\mathcal{O}$	α	Control output	$F\ (s_1=s_4=0)$	$F\ (s_1=0,s_4=1)$
	$\pi/2$	$\|0\rangle_c\equiv\|\ell\rangle_{\mathbf{k}_B}$	0.932 ± 0.004	0.959 ± 0.003
1		$\|1\rangle_c=\|r\rangle_{\mathbf{k}_B}$	0.941 ± 0.005	0.940 ± 0.005
	$\pi/4$	$\|0\rangle_c=\|\ell\rangle_{\mathbf{k}_B}$	0.919 ± 0.007	0.932 ± 0.007
		$\|1\rangle_c=\|r\rangle_{\mathbf{k}_B}$	0.878 ± 0.009	0.959 ± 0.006

$R_z(\alpha)|+\rangle=\frac{e^{-i\alpha/2}}{\sqrt{2}}(|0\rangle+e^{i\alpha}|1\rangle)]$ and control qubit $|0\rangle$, $|1\rangle$, or $|\pm\rangle$ depending on the measurement basis of qubit 1.

The experimental realization of this gate is performed by adopting the following ordering between the physical qubits:

$$\text{(c)}\quad (1,2,3,4)=(\mathbf{k}_A,\mathbf{k}_B,\pi_B,\pi_A),$$

$$\mathcal{U}=\sigma_z H\otimes\sigma_x\otimes\mathbb{1}\otimes H. \tag{24}$$

In this case the control output qubit is encoded in the momentum $\mathbf{k_B}$, while the target output is encoded in the polarization π_B. In order to compensate the H_t gate arising from the cluster algorithm we inserted two Hadamard in the polarization analysis of the detectors b_1 and b_2 (see Fig. 5). The output state in the laboratory basis is then written as

$$|\Psi_{out}\rangle=(\Sigma)^{s_4}\sigma_x^{(c)}\mathcal{G}_{\mathrm{CNOT}}(\mathcal{O}\sigma_z^{s_1}|+\rangle_c\otimes R_z(\alpha)|+\rangle_t), \tag{25}$$

where all the possible measurement outcomes of qubits 1 and 4 are considered. The Pauli errors are $\Sigma=\sigma_z^{(c)}\sigma_z^{(t)}$, while the matrix $\sigma_x^{(c)}$ is due to the changing between cluster and laboratory basis.

By measuring $\mathbf{k_A}$ in the basis $\{|\ell\rangle_{\mathbf{k_A}},|r\rangle_{\mathbf{k_A}}\}$ we perform the $\mathcal{O}=H$ operation on the control qubit. By looking at Eq. (25), this means that if $s_{\mathbf{k_A}}\equiv s_1=0$ ($s_{\mathbf{k_A}}=1$) the control qubit is $|1\rangle$ ($|0\rangle$), while the target qubit is $R_z(\alpha)|+\rangle_t$ ($\sigma_xR_z(\alpha)|+\rangle_t$). In this case the gate acts on a control qubit $|0\rangle$ or $|1\rangle$, without any superposition of these two states. We first verified that the gate acts correctly in this situation. In Table IV (top) we report the experimental fidelities (F) of the output target qubit π_B for two different values of α and for the two possible values of s_4. The high values of F show that the gate works correctly when the control qubit is $|0\rangle$ or $|1\rangle$.

In the second step we verified that the gate works correctly with the control qubit in a superposition of $|0\rangle$ and $|1\rangle$. This was realized by measuring the qubit $\mathbf{k_A}$ in the basis $|\pm\rangle_{\mathbf{k_A}}$ and performing the $\mathcal{O}=\mathbb{1}$ operation on the control qubit. The output state is written (without errors) as $|\Psi_{out}\rangle=|1\rangle_c\otimes R_z(\alpha)|+\rangle_t+|0\rangle_c\otimes\sigma_xR_z(\alpha)|+\rangle_t$. In Table IV (bottom) we show the values of the experimental fidelities of the target qubit π_B, corresponding to the measurement of the output

TABLE V. Experimental fidelity (F) of CPHASE gate output target qubit for different value of α and β. In parentheses we indicate the corresponding measured output of the control qubit $\mathbf{k_A}$.

α	β	$F_{\mathbf{k}_B}(\mathbf{k_A}=\|-\rangle)$	$F_{\mathbf{k}_B}(\mathbf{k_A}=\|+\rangle)$
0	0	0.878 ± 0.004	0.933 ± 0.003
π	0	0.919 ± 0.003	0.917 ± 0.004
$\pi/2$	0	0.876 ± 0.005	0.816 ± 0.005
$-\pi/2$	0	0.880 ± 0.004	0.883 ± 0.004
$\pi/2$	$\pi/2$	0.969 ± 0.002	0.949 ± 0.003
$\pi/2$	$-\pi/2$	0.950 ± 0.003	0.939 ± 0.003
$\pi/4$	$\pi/2$	0.885 ± 0.006	0.916 ± 0.005

control qubit $\mathbf{k_B}$ in the basis $\{|0\rangle,|1\rangle\}$ when $\mathcal{O}=\mathbb{1}$. These results demonstrate the high quality of the operation also in this case.

C. CPHASE gate

The four-qubit cluster allows also the realization of a CPHASE gate for arbitrary target qubit and fixed control $|+\rangle_c$. The measurement pattern needed for this gate is shown in Fig. 9 (bottom) and consists of the measurements of qubits 1 and 2 in the bases $B_1(\alpha)$ and $B_2[(-1)^{s_1}\beta]$. These two measurements realize a generic rotation $R_x(\beta)R_z(\alpha)$ on the input target qubit $|+\rangle_t$, as explained in Sec. IV A. The link existing between qubit 3 and 4 in the cluster performs the subsequent CPHASE gate between the control qubit $|+\rangle_c$ and a generic target qubit $R_x(\beta)R_z(\alpha)|+\rangle_t$.

The experimental realization is done by considering the following ordering between the physical qubits:

$$\text{(d)}\quad (1,2,3,4)=(\pi_A,\pi_B,\mathbf{k}_B,\mathbf{k}_A),$$

$$\mathcal{U}=H\otimes\mathbb{1}\otimes\sigma_x\otimes\sigma_z H. \tag{26}$$

We realized a CPHASE gate for arbitrary target qubit and fixed control $|+\rangle_c$ [see Fig. 9(c)] by measuring qubits 1 and 2 of $|\Phi_4^{\text{lin}}\rangle$ in the bases $|\alpha_\pm\rangle$ and $|(-)^{s_1}\beta_\pm\rangle$, respectively. By considering ordering (d) we encoded the output state in the physical qubits $\mathbf{k}_A$ and $\mathbf{k}_B$. For $s_1=s_2=0$, by using the appropriate base changing, the output state is written as

$$|\Psi_{out}\rangle=|-\rangle_{\mathbf{k}_A}\otimes\sigma_x|\Phi\rangle_{\mathbf{k}_B}+|+\rangle_{\mathbf{k}_A}\otimes\sigma_x\sigma_z|\Phi\rangle_{\mathbf{k}_B}. \tag{27}$$

Here $|\Phi\rangle_{\mathbf{k}_B}=R_x(\beta)R_z(\alpha)|+\rangle$ and the matrix σ_x is due to the change of basis. We show in Table V the measured fidelities of the target $\mathbf{k}_B$ corresponding to a control $|+\rangle_{\mathbf{k}_A}$ ($|-\rangle_{\mathbf{k}_A}$) for different values of α and β. An average fidelity $F=0.907\pm0.010$ and $F=0.908\pm0.011$ was obtained in the two cases.

V. ALGORITHMS

A. Grover's algorithm

The Grover's search algorithm for two input qubits is implemented by using the four-qubit cluster state [5,8,29,30].

Let us describe the algorithm in general. Suppose to have 2^M elements (encoded in M qubits) and a black box (or oracle) that tags one of them. The tagging, denoted as $\mathcal{T}$, is realized by changing the sign of the desired element. The goal is to identify the tagged item by a repeated query to the black box; the Grover's algorithm requires $\mathcal{O}(\sqrt{2^M})$ operations, while the best classical algorithm takes on average $2^M/2$ calculations.

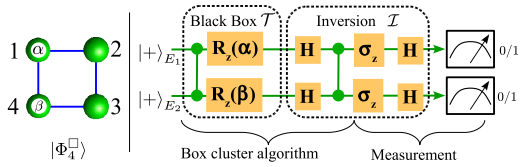

FIG. 10. (Color online) Grover's algorithm. Left: Realization of the Grover's algorithm through the measurements of qubit 1 and 4 on the box cluster $|\Phi_4^{\square}\rangle$. Right: Logical circuit implementing the Grover operator $G=\mathcal{I}\mathcal{T}$. The first part of G is implemented by the cluster algorithm while the second part by the measurement.

The general algorithm starts with the input state prepared as $|\Psi^+\rangle\equiv|+\rangle_{E_1}\cdots|+\rangle_{E_M}$ and consists of repeated applications of the Grover operator G, given by the oracle tagging $\mathcal{T}$ followed by the so-called *inversion about average* operation $\mathcal{I}\equiv2|\Psi^+\rangle\langle\Psi^+|-\mathbb{1}$. We can thus write $G\equiv\mathcal{I}\mathcal{T}$. In general, after $R=\mathcal{O}(\sqrt{2^M})$ iterations of G the tagged item is obtained at the output of the circuit with high probability.

In the case of 2 qubits the quantum algorithm [shown in Fig. 10 (right)] requires just one G operation. The four elements are $|0\rangle_{E_1}|0\rangle_{E_2}$, $|0\rangle_{E_1}|1\rangle_{E_2}$, $|1\rangle_{E_1}|0\rangle_{E_2}$, and $|1\rangle_{E_1}|1\rangle_{E_2}$. They are prepared in a complete superposition, i.e., in the state $|+\rangle_{E_1}|+\rangle_{E_2}$, while the black box tagging acts simply by changing the sign to one of the elements, for instance $|1\rangle|0\rangle\rightarrow-|1\rangle|0\rangle$. It consists of a CPHASE gate followed by two single qubit rotations, $R_z(\alpha)_1$ and $R_z(\beta)_2$. By setting the rotation angles $\alpha\beta$ to 00, $\pi0$, 0π, or $\pi\pi$ the black box tags, respectively the states $|1\rangle|1\rangle$, $|1\rangle|0\rangle$, $|0\rangle$, $|1\rangle$, or $|0\rangle|0\rangle$ [remember that $R_z(\pi)$ is σ_z up to a global phase]. The inversion operation consists of a CPHASE gate and single qubit gates [see Fig. 10 (right)]. The inversion acts such as the output state of the system is exactly the tagged item.

This algorithm can be realized in the one-way model by using the four-qubit box cluster state. By measuring qubit 1 and 4 in the basis $B_1(\alpha)$ and $B_4(\beta)$ we implement the black box and the first part of the inversion algorithm (*box cluster algorithm* in Fig. 10). The output qubits are then encoded into the physical qubit 2 and 3. The $H\sigma_z$ operation needed to conclude the inversion operation can be performed at the measurement stage. Indeed we can measure the qubit 2 and 3 in the basis $B_j(\pi)$: this is equivalent to apply $H\sigma_z$ gates and then to perform the measurement in the computational basis $\{|0\rangle,|1\rangle\}$ (see *measurement* in Fig. 10).

Without Pauli errors the desired tagged item is given by $|s_2\rangle|s_3\rangle$. Depending on the measurement outcome (s_1 and s_4) the corresponding Pauli errors are $(\sigma_z)^{s_1}(\sigma_x)^{s_4}$ on the qubit E_1 and $(\sigma_z)^{s_4}(\sigma_x)^{s_1}$ on the qubit E_2. However, since the output of the algorithm will be one of the four states of computational basis, the σ_z operation leaves the output unchanged, while σ_x flips the output state [see Eq. (12)]. In this way the tagged item is found to be $|s_2\oplus s_4\rangle_{E_1}|s_3\oplus s_1\rangle_{E_2}$ and the FF corrections are simply relabeling FF.

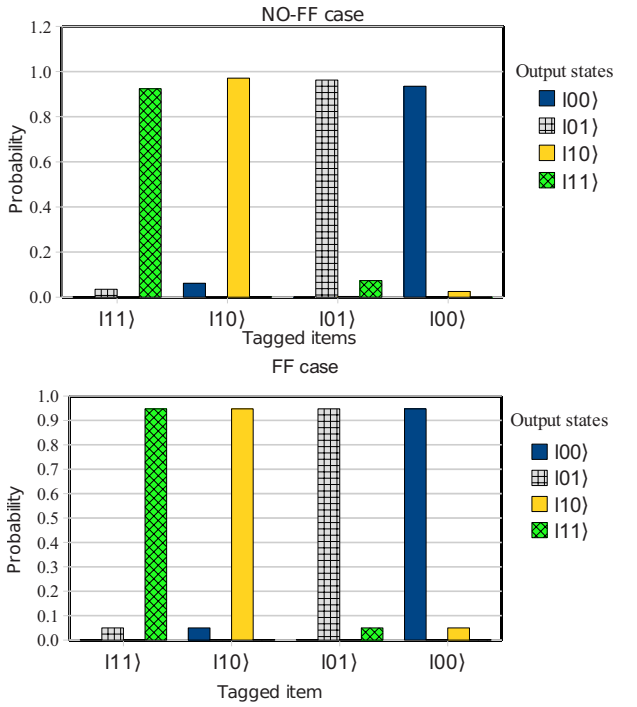

FIG. 11. (Color online) Experimental results of the Grover's algorithm. Upper graph: We report, for different tagged items, the probability of the different output states when the computation proceeds without Pauli errors. Experimental errors are of the order of 0.005 for higher histograms, while for the lower ones becomes 0.0005. Lower graph: Experimental probabilities in the FF case. Experimental errors are of the order of 0.002 for higher histograms, while for the lower ones becomes 0.0004. Each datum is obtained by 10 s measurement.

Let us now describe the experimental realization of the Grover's algorithm by our apparatus. If we consider the following ordering of the physical qubits [see Eq. (15)]:

$$\text{(e)} \quad (1,2,3,4) = (\mathbf{k}_B, \pi_A, \mathbf{k}_A, \pi_B),$$

$$\mathcal{U} = \sigma_x H \otimes H \otimes \sigma_z H \otimes H, \tag{28}$$

the generated state (14) is equivalent to the box cluster $|\Phi_4^{\square}\rangle$ up to the single qubit unitaries given by $\mathcal{U}$. By this change of basis we can determine the correct measurement to be performed in the laboratory basis.

The experimental results are shown in Fig. 11. In the upper graph we show the experimental fidelities obtained when the computation proceeds without Pauli errors, i.e., $s_1 = s_4 = 0$. The mean value of probability of identifying the tagged item is 0.9482 ± 0.0080 and the algorithm is realized at ~ 250 Hz. We report in the lower graph the identification probability with FF corrections implemented. In this case the tagged item is discovered with probability 0.9475 ± 0.0022 and the algorithm is realized at ~ 1 kHz repetition rate, as expected. Note that in the lower graph a change of the tagged item corresponds to reorder the histograms. This is due to the fact that the measurement in the basis $B(\pi) = \{|-\rangle, |+\rangle\}$ is the same as $B(0) = \{|+\rangle, |-\rangle\}$: the difference is that in the first case we associate $s=0$ to $|-\rangle$ while in the second we associate $s=0$ to $|+\rangle$.

B. Deutsch's algorithm

The four-qubit cluster state allow the implementation of the Deutsch's algorithm for two input qubits [31]. This algorithm distinguishes two kinds of functions $f(x)$ acting on a generic M-bit query input: the *constant* function returns the same value (0 or 1) for all input x and the *balanced* function gives 0 for half of the inputs and 1 for other half. Usually the function is implemented by a black box (or oracle). By the Deutsch's algorithm one needs to query the oracle just once, while by using deterministic classical algorithms one needs to know the output of the oracle many times (as $2^{M-1}+1$). The oracle implements the function f on the query input $|x\rangle_q$ through an ancillary qubit $|y\rangle_e$:

$$\text{Oracle:} |x\rangle_q |y\rangle_e \to |x\rangle_q |y \oplus f(x)\rangle_e, \tag{29}$$

where $y=0,1$ and $x=0,1,\ldots,2^M-1$. If the oracle acts on the input qubits $|+\rangle_1 |+\rangle_2 \cdots |+\rangle_M |-\rangle_e$, the output state is

$$\frac{1}{\sqrt{2^M}} \sum_{x=0}^{2^M-1} (-1)^{f(x)} |x\rangle_q |-\rangle_e. \tag{30}$$

By applying the Hadamard gates for each qubits the output state can be written as

$$\begin{cases} \bigotimes_{a=1}^{M} |0\rangle_a |1\rangle_e, & \text{if } f \text{ is constant,} \\ \bigotimes_{a=1}^{M} |1\rangle_a |1\rangle_e, & \text{if } f \text{ is balanced.} \end{cases} \tag{31}$$

Then, by measuring the query state in the computational basis, we can discover if the function f is constant or balanced. The algorithm thus proceeds through the following three steps:

(1) *Preparation*. It consists in the initialization of the input state into $|+\rangle_1 |+\rangle_2 \cdots |+\rangle_M |-\rangle_e$.

(2) *BB*. This is the Oracle operation (29).

(3) *Readout*. This corresponds to apply the Hadamard gates for each qubits and measure them in the computational basis $\{|0\rangle, |1\rangle\}$.

In the two-qubit version the function f acts on a single qubit $|x\rangle_q$. In this case there are four possible functions f on a single qubit: two are constant, namely $f_1(0) = f_1(1) = 0$ and $f_2(0) = f_2(1) = 1$, while two are balanced $f_3(0) = 0$, $f_3(1) = 1$ and $f_4(0) = 1, f_4(1) = 0$. Let us describe the oracle operation (29) as a "black box" (BB). In Table VI we give the oracle operation on the two qubits $|x\rangle_q |y\rangle_e$ depending on the chosen function f_i.

By the four-qubit cluster it is possible to implement the two-qubit version of the algorithm. Let us consider Fig. 12. The algorithm is implemented by the measurements of qubit 2 and 4, while the output is encoded in the qubit 1 (query qubit) and 3 (ancillary qubit). Precisely, the measurement of qubit 4 in the basis $B_4(\pi)$ performs the transformation $HR_z(\pi)$ on the ancillary qubit.

TABLE VI. Oracle operation (BB) depending on the single qubit function f_i. The two function f_1 and f_2 are constant, while f_3 and f_4 are balanced.

	Constant functions		Balanced functions	
	f_1	f_2	f_3	f_4
BB	$\mathbb{1}_a \otimes \mathbb{1}_e$	$\mathbb{1}_a \otimes \sigma_x^{[e]}$	$\mathcal{G}_{\mathrm{CNOT}_{ae}}$	$(\mathbb{1}_a \otimes \sigma_x^{[e]})\mathcal{G}_{\mathrm{CNOT}_{ae}}$

The BB is implemented by the measurement of qubit 2. If the oracle chooses the measurement basis $\{|0\rangle_2, |1\rangle_2\}$ it implements the f_1 function. In fact qubit 2 is removed from the cluster and no operation is performed on the other qubits. The full cluster algorithm consists of the operation $\mathbb{1}_q \otimes [HR_z(\pi)]_e$. This is exactly the Deutsch algorithm in the case of constant function up to a Hadamard gate on the query qubit that must be implemented in the final measurement step. The measurement basis on the output qubits 1 and 3 are then $B_1(0)$ and $\{|0\rangle_3, |1\rangle_3\}$ (see *measurement* in Fig. 12).

By choosing $B_2(\frac{\pi}{2})$ as measurement basis for qubit 2 the oracle implements the f_3 function and the obtained operation is (see CBB_3) $[R_z(-\frac{\pi}{2})]_q \otimes [R_z(-\frac{\pi}{2})]_e \mathcal{G}_{\mathrm{CZ}_{qe}}$. Together with the $\mathbb{1}_q \otimes [HR_z(\pi)]_e$ the full cluster algorithm becomes $[R_z(-\frac{\pi}{2})]_q \otimes [R_z(-\frac{\pi}{2})H]_e (\mathcal{G}_{\mathrm{CNOT}_{qe}})\, \mathbb{1}_q \otimes [R_z(\pi)]_e$ (the cluster algorithm in Fig. 12). This corresponds to the Deutsch's algorithm in case of balanced function up to $[R_z(-\frac{\pi}{2})]_q \otimes [R_z(-\frac{\pi}{2})H]_e$ to be corrected in the final measurement step. These corrections corresponds to the choice of the measurement basis on the output qubits 1 and 3 as $B_1(-\frac{\pi}{2})$ and $\{|0\rangle_3, |1\rangle_3\}$ (see *measurement* in Fig. 12).

Without Pauli errors the output state of the Deutsch's algorithm is given by $|s_1=0\rangle_q |s_3=1\rangle_e$ in case of f_1 and $|s_1=1\rangle_q |s_3=1\rangle_e$ in case of f_3 [see Eq. (31)]. The correct outcomes considering the Pauli errors are in this case

$$|s_1 \oplus s_2\rangle_q |s_3 \oplus s_4\rangle_e, \quad \text{for } f_1,$$

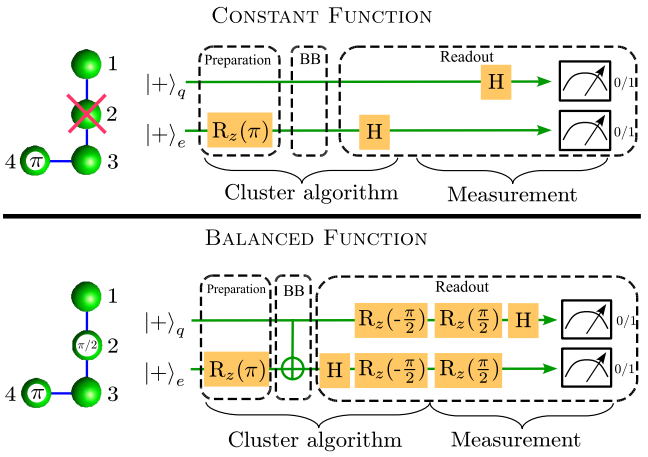

FIG. 12. (Color online) Implementation of the Deutsch's algorithm. Measurement pattern on the physical cluster (left) and corresponding operations on the logical qubits (right). Measurements of qubit 2 and 4 on the left correspond to the *cluster algorithm* in the right. The output logical qubits are encoded in the physical qubits 1 (query, q) and 3 (ancilla, e) that should be measured in order to read out the answer of the algorithm (*measurement* in the right).

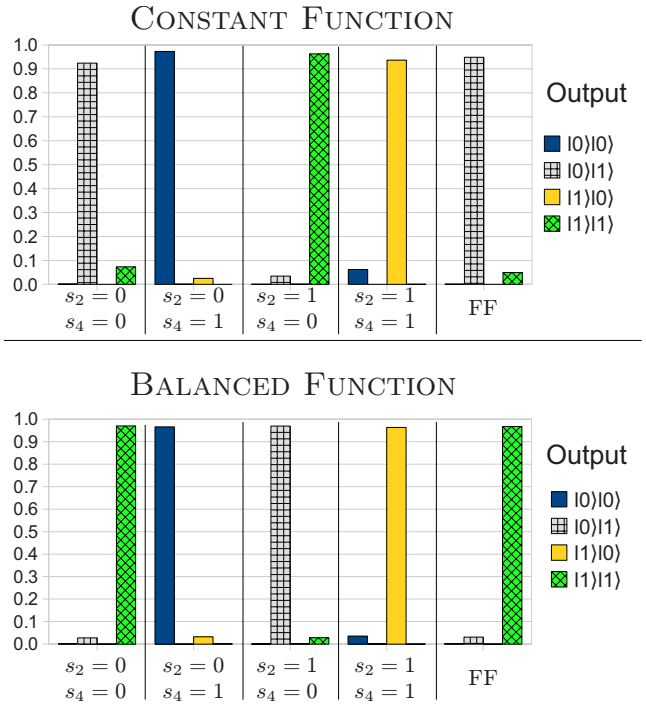

FIG. 13. (Color online) Experimental probabilities of the output states of the Deutsch algorithm in case of constant (top) or balanced (bottom) function. The probabilities are shown for all the values of s_4 and s_2, while in the last column are shown the results after the FF relabeling operation.

$$|s_1 \oplus s_2 \oplus s_4\rangle_q |s_3 \oplus s_4\rangle_e, \quad \text{for } f_3. \tag{32}$$

Note that the BB operation obtained by the function f_2 (f_4) is essentially the same, up to a global phase, with respect to the function f_1 (f_3). In the following we then show only the results obtained in the case of f_1 and f_3.

We show in Fig. 13 the experimental probabilities of the different output states as a function of the value of s_2 and s_4 for the f_1 and f_3 case. In the case of f_1, for $s_2=s_4=0$ the output of the algorithm is the state $|0\rangle_q |1\rangle_e$ with probability 0.924 ± 0.005, while in the other cases are $|0 \oplus s_2\rangle_q |1 \oplus s_4\rangle_e$ in agreement with Eq. (32). By using the FF relabeling we obtain the correct output with probability 0.949 ± 0.002. In the case of balanced function the correct output after the FF operation is obtained with probability 0.967 ± 0.002.

VI. CONCLUSIONS

We have described the basic principles of operation of a one-way quantum computer operating with cluster states built with two photons entangled in two different DOF's. We have also presented the experiment (and the corresponding results) carried out when the DOF's are the polarization and the linear momentum.

One-way QC based on multi-DOF cluster states presents some important advantages with respect to the one performed with multiphoton cluster states. In particular the repetition rate of computation is almost three order of magnitude larger; the fidelity of the computational operations is much higher (nearly 90%, even with active FF); in some

cases the intermediate FF operations do not require active modulators, differently from the case of multiphoton cluster states; the FF operations are automatically (and also deterministically) implemented in these cases because of the entanglement existing between the two DOF's of the same particle; working with two photons allows to minimize the problems caused by the limited efficiency of single photon detectors.

The possibility of multi-DOF encoding of qubits is a useful and powerful tool for an optical approach to quantum computation. By detecting a single photon we measure at the same time different qubits. A simultaneous collapse of some qubits can be caused by either a measurement process or an environment perturbation acting on a single photon. In presence of noise this corresponds to loosing these qubits. On the other hand, as explained in the text, this feature can be used to deterministically implement the FF measurements.

A larger number of qubits is necessary to perform more complex gates and algorithms. For instance, using a type-I NL crystal a continuum of **k**-emission modes is virtually available to create a multiqubit spatial entangled state. Even if the number of modes scales exponentially with the number of qubits, it is still possible to obtain a reasonable number (six or even eight) of qubits. In a recent experiment we tested a reliable interferometric configuration to implement energy-time entanglement as a further independent DOF in a two-photon cluster state [32]. Hence, increasing the number of DOF's of the photons allows one to move further than what is expected by increasing the number of photons. Because of all these reasons we believe that cluster states based on many DOF's is a good alternative for experimental QC with photons on a midterm perspective.

ACKNOWLEDGMENT

This work was supported by Finanziamento Ateneo 06, Sapienza Università di Roma.

[1] R. Raussendorf and H. J. Briegel, Phys. Rev. Lett. **86**, 5188 (2001).
[2] M. A. Nielsen, Phys. Rev. Lett. **93**, 040503 (2004).
[3] D. E. Browne and T. Rudolph, Phys. Rev. Lett. **95**, 010501 (2005).
[4] N. Kiesel, C. Schmid, U. Weber, G. Tóth, O. Gühne, R. Ursin, and H. Weinfurter, Phys. Rev. Lett. **95**, 210502 (2005).
[5] P. Walther, K. J. Resch, T. Rudolph, E. Schenck, H. Weinfurter, V. Vedral, M. Aspelmeyer, and A. Zeilinger, Nature (London) **434**, 169 (2005).
[6] T. P. Bodiya and L.-M. Duan, Phys. Rev. Lett. **97**, 143601 (2006).
[7] V. Danos and E. Kashefi, Phys. Rev. A **74**, 052310 (2006).
[8] R. Prevedel, P. Walther, F. Tiefenbacher, P. Böhi, R. Kaltenbaek, T. Jennewein, and A. Zeilinger, Nature (London) **445**, 65 (2007).
[9] S. Popescu, Phys. Rev. Lett. **99**, 250501 (2007).
[10] M. Varnava, D. E. Browne, and T. Rudolph, Phys. Rev. Lett. **100**, 060502 (2008).
[11] C.-Y. Lu, X.-Q. Zhou, O. Gühne, W.-B. Gao, J. Zhang, Z.-S. Yuan, A. Goebel, T. Yang, and J.-W. Pan, Nat. Phys. **3**, 91 (2007).
[12] A. Cabello, Phys. Rev. Lett. **95**, 210401 (2005).
[13] V. Scarani, A. Acin, E. Schenck, and M. Aspelmeyer, Phys. Rev. A **71**, 042325 (2005).
[14] G. Vallone, E. Pomarico, P. Mataloni, F. De Martini, and V. Berardi, Phys. Rev. Lett. **98**, 180502 (2007).
[15] M. Nielsen and I. Chuang, *Quantum Computation and Quantum Information* (Cambridge University Press, Cambridge, 2000).
[16] E. Knill, R. Laflamme, and G. J. Milburn, Nature (London) **409**, 46 (2001).
[17] P. Kok, W. J. Munro, K. Nemoto, T. C. Ralph, J. P. Dowling, and G. J. Milburn, Rev. Mod. Phys. **79**, 135 (2007).
[18] M. Barbieri, C. Cinelli, P. Mataloni, and F. De Martini, Phys. Rev. A **72**, 052110 (2005).
[19] M. Barbieri, F. De Martini, P. Mataloni, G. Vallone, and A. Cabello, Phys. Rev. Lett. **97**, 140407 (2006).
[20] G. Vallone, E. Pomarico, F. De Martini, and P. Mataloni, Phys. Rev. Lett. **100**, 160502 (2008).
[21] G. Vallone, E. Pomarico, F. De Martini, and P. Mataloni, Laser Phys. Lett. **5**, 398 (2008).
[22] K. Chen, C.-M. Li, Q. Zhang, Y.-A. Chen, A. Goebel, S. Chen, A. Mair, and J.-W. Pan, Phys. Rev. Lett. **99**, 120503 (2007).
[23] M. A. Nielsen, e-print arXiv:quant-ph/0504097v2, Rev. Math. Phys. (to be published).
[24] M. S. Tame, M. Paternostro, M. S. Kim, and V. Vedral, Phys. Rev. A **72**, 012319 (2005).
[25] R. Raussendorf, D. E. Browne, and H. J. Briegel, Phys. Rev. A **68**, 022312 (2003).
[26] C. Cinelli, M. Barbieri, R. Perris, P. Mataloni, and F. De Martini, Phys. Rev. Lett. **95**, 240405 (2005).
[27] D. Gottensman, Ph.D. thesis, CalTech, Pasadena, 1997.
[28] M. Hein, W. Dür, J. Eisert, R. Raussendorf, M. V. den Nest, and H.-J. Briegel, in *Quantum computers, algorithms and chaos*, edited by P. Zoller, G. Casati, D. Shepelyansky, and G. Benenti (International School of Physics Enrico Fermi, Varenna, Italy (2006).
[29] L. K. Grover, Phys. Rev. Lett. **79**, 325 (1997).
[30] L. K. Grover, Phys. Rev. Lett. **79**, 4709 (1997).
[31] M. S. Tame, R. Prevedel, M. Paternostro, P. Bohi, M. S. Kim, and A. Zeilinger, Phys. Rev. Lett. **98**, 140501 (2007).
[32] A. Rossi, G. Vallone, F. De Martini, and P. Mataloni, Phys. Rev. A **78**, 012345 (2008).
[33] Note that the usual postselection needed to select out the vacuum state is in any case necessary. This is unavoidable since SPDC is a not deterministic process.
[34] This is a generic rotation iff the input state $|\chi_{in}\rangle$ is not $|0\rangle$ or $|1\rangle$. In our case the algorithm is implemented with $|\chi_{in}\rangle=|\pm\rangle$. In fact three sequential rotations are in general necessary to implement a generic SU(2) matrix but only two, namely $R_x(\beta)R_z(\alpha)$, are sufficient to rotate the input state $|\chi_{in}\rangle=|\pm\rangle$ into a generic state